Towards the Prediction of the Transport Properties of Cluster-Based Molybdenum Chalcogenides

Rabih Al Rahal Al Orabi,[ac] Benoît Boucher,[a] Bruno Fontaine,[a] Philippe Gall,[a] Christophe Candolfi,[b] Bertrand Lenoir,[b] Patrick Gougeon,[a] Jean-François Halet[a] and Régis Gautier[a]*

[a]*Institut des Sciences Chimiques de Rennes, UMR 6226 CNRS – Université de Rennes 1 – INSA de Rennes – Ecole Nationale Supérieure de Chimie de Rennes, 11 allée de Beaulieu, CS 50837, 35708 Rennes Cedex, France.*

E-mail: rgautier@ensc-rennes.fr

[b]*Institut Jean Lamour, UMR 7198 CNRS – Université de Lorraine, Parc de Saurupt, CS 50840, 54011 Nancy, France*

[c]*Present address: Advanced Polymers & Materials Department (ARTI/APMD) AXEL'ONE Collaborative Platform - Innovative Materials, 87 rue des frères Perret – BP62, 69192 Saint FONS Cedex.*

Electronic supplementary information (ESI) available (Two figures).

Abstract

Molybdenum cluster chemistry is one of the richest series of cluster-based materials with nuclearities up to 40. Among them, molybdenum chalcogenides are promising materials for high-temperature thermoelectric applications due to their intrinsic, extremely low thermal conductivities. In this paper, we studied the electronic transport properties of three selenides based on octahedral Mo_6 and bioctahedral Mo_9 motifs using band structure calculations and a semi-classical approach. The electronic structure of these materials is governed by the cluster units. Unlike the electronic conductivity, the computed thermopower hardly depend on the structural details suggesting that such a computational approach may be useful to identify new interesting candidates for thermoelectric applications among cluster-based materials.

1 Introduction

Since the end of the 90s, the Chevrel phases of general formula $M_xMo_6Q_8$ (M = transition metal or rare-earth metal, x = 0-4, and Q = S, Se, or Te) have been investigated for their thermoelectric properties.[1-7] These compounds based on face-capped octahedral Mo_6Q_8 units were considered as promising candidates for electrical power generation because of their ability to accommodate metal cations that can cause effective phonon scattering, thus reducing significantly their lattice thermal conductivity.[8] Indeed, the amount x of metal cations modifies the electron count that governs the electrical properties of these materials. This degree of freedom provides a simple fine-tuning parameter of the electron count to optimize their electrical resistivity (ρ) and thermopower (α). These electrical properties, combined with inherently very low thermal conductivity (κ), raised exciting prospects to achieve high dimensionless thermoelectric figure of merit $ZT = \alpha^2 T/\rho\kappa$. To date, the highest performances were achieved for the Chevrel phase $Cu/FeMo_6Se_8$ with a peak ZT value close to 0.6 at 1150 K.[2]

Recently, the related family of chalcogenides based on bioctahedral Mo_9 clusters were also studied for their transport properties. Both $Ag_xMo_9Se_{11}$ ($3.4 \leq x \leq 3.9$) and $Ag_2Tl_2Mo_9Se_{11}$ possess ZT values that surpass those of the above-mentioned Chevrel phases, reaching 0.65 at 800 K.[9-12] A few additional compounds based on octahedral Mo_6 and/or related Mo_9 and Mo_{12} clusters also exhibit interesting thermoelectric properties at high temperatures.[13,14] Most of them show the remarkable ability to poorly conduct heat, a property which is at the core of the relatively high ZT values achieved near 800 K. These results are very promising overall since they may be enhanced *via* either optimization of the nature and nominal content of the cations, through substitutions on the Mo or Se sites, or by nanostructuring.[15,16]

Many other molybdenum cluster-based materials have been synthesized over the last decades. Various nuclearities ranging from 2 to more than 40 metal atoms, and various topologies have been observed in oxides, chalcogenides and halides.[17,18] Identifying materials with promising thermoelectric properties among these cluster compounds requires measurements of their transport properties. This, in turn, necessitates the synthesis of a significant amount of materials to obtain bulk dense samples needed for accurate measurements. In addition, identification of successful dopants is usually performed on an experimental trial-and-error basis. Because all of these experimental requirements are often very difficult and time-consuming, alternative approaches based on first-principles calculation methods are currently used to identify and predict the transport properties of promising thermoelectric materials. A wealth of literature data has demonstrated the power of these first-principles modelling approaches based on density functional theory (DFT) in understanding thermoelectric properties and defect characteristics of diverse materials.[19-25] DFT and electronic transport properties computations enable in turn rapidly generating large amounts of data that allow high-throughputs methods.[26,27] However, one of the main limitations of these fast *in silico* methods is related to the approximation of the electronic relaxation time and thermal conductivity which are held constant even across diverse compounds.

In this work, we aim at computing the transport properties of cluster-based compounds within the framework of DFT and a semi-classical approach (Boltzmann equation). The results are compared with the experimental data available for these compounds.[9-14] We will focus our study on three compounds, namely $Ag_xMo_9Se_{11}$ ($3.4 \leq x \leq 3.9$), $Ag_2Tl_2Mo_9Se_{11}$, and $Ag_3In_2Mo_{15}Se_{19}$, the transport properties of which were reported in our previous works.[9-14] The objectives are two-fold. First, models of the crystal structure should be considered to account for the inherent disorder present in these compounds on the interstitial cations (Ag, In, Tl). We thus search to understand the influence of a given model on the electronic band

structures and on the computed transport properties. Second, these calculations should help in identifying which transport property of cluster-based materials can be satisfactorily predicted using such an approach.

2 Methods

Density functional theory (DFT) calculations were performed using the WIEN2k program package.[28] Geometry optimizations were carried out using the generalized gradient approximation (GGA) exchange-correlation functional within the parameterization of Perdew, Burke and Ernzerhof (PBE).[29] Because GGA exchange-correlation functionals are known to underestimate experimental band gaps, the modified Becke-Johnson (mBJ) functional proposed by Tran and Blaha was also utilized.[30] This functional yields band gaps with an accuracy similar to hybrid functional or GW methods, but are obtained at considerable reduced computational cost. A plane-wave cutoff corresponding to $R_{MT}K_{max} = 7$ was used, and the radial wave-functions inside the nonoverlapping muffin-tin spheres surrounding the atoms were expanded up to $l_{max} = 12$. The charge density was Fourier expanded up to the reciprocal vector $G_{max} = 14$ Å^{-1}. Total energy convergence was achieved with respect to the Brillouin zone (BZ) integration using a mesh of 500 *k*-points, which generated 84 *k*-points in the irreducible BZ part. Electronic bands and density of states (DOS) were shifted in order that the Fermi level ε_F lies at 0 eV.

Electronic transport coefficients were calculated within the Boltzmann Transport Equation (BTE) with a constant relaxation time τ for the electrons and the rigid band structure approximation,[31,32] [1]as implemented in the BoltzTrap-1.2.5 code.[33] Electrical conductivity and power factor were calculated with respect to τ, while the thermopower is independent of τ. 10000 *k*-points in the BZ were used to compute the band derivatives and density of states for the transport calculations.

3 Results and discussion

3.1 $Ag_xMo_9Se_{11}$ ($3.4 \leq x \leq 3.9$)

The $Ag_xMo_9Se_{11}$ compounds crystallize in the orthorhombic space group *Cmcm*.[34] The building block is the bioctahedral $Mo_9Se^i_{11}Se^a_6$ cluster unit shown in Fig. 1, where Se^i atoms are capping triangular faces of the Mo_9 motifs and Se^a atoms are connected to Mo atoms of the outer Mo_3 triangles of the Mo_9 motif. Each Mo_9 unit is linked to 8 other Mo_9 units *via* Mo-Se^{i-a} bonds. The three-dimensional network formed by these clusters leaves empty channels that accommodate the Ag atoms delocalized over four crystallographically independent sites (Fig 1 and Table 1). Pioneer works on $Ag_xMo_9Se_{11}$ single crystals prepared by chemical vapour transport led to x values limited to the range 3.6 – 3.76.[8] Later, single-phase polycrystalline samples were obtained for $3.4 \leq x \leq 3.9$ allowing for a detailed study of their high-temperature thermoelectric properties as a function of Ag content.[34] X-ray diffraction studies further demonstrated that increasing the Ag concentration from x = 3.4 to 3.9 results in an increase in the unit cell volume.

The electronic structure of Mo_9-based cluster compounds has been studied using semi-empirical and first-principles approaches.[35-42] In most cases, the electronic structure of these compounds can be rationalized on the basis of the molecular orbital (MO) diagram of the building unit Mo_9Q_{11} cluster (Q = chalcogen). It is characterized by a large energy separation between Mo-Mo bonding and Mo-Mo antibonding MOs leading to a substantial HOMO/LUMO gap for the charged $Mo_9Q_{11}^{4-}$ anion. For this optimal charge, the highest MOs exhibit an overall Mo-Mo nonbonding character. As a consequence, the main interatomic distances within the $[Mo_9Q_{11}]^{n-}$ unit hardly change when their geometry is optimized for different charges n.[36] This feature is also observed in the crystal structure of Mo_9-based compounds where the metallic electron (ME) count, *i.e.*, electrons available for metal-metal bonding, can vary between 32 to 36 per $Mo_9Q_{11}^{n-}$ motif (n = 0-4). For instance, the ME count

of the Mo_9 unit present in *h*-Mo_9Se_{11}, $Ag_{4.1}ClMo_9Se_{11}$ and $Ag_{2.6}CsMo_9Se_{11}$ is equal to 32, 35.1 and 35.6, respectively. The averaged Mo-Mo distances in these compounds are similar, equal to 2.731 Å, 2.693 Å and 2.694 Å, respectively. Periodic DFT calculations confirmed that the electronic structure of these three compounds can be deduced from that of the Mo_9 motifs since inter-cluster interactions are not strong enough to alter the MO pattern of the Mo_9 cluster and interactions of interstitial atoms with the Mo-Se network are mainly electrostatic in character.[39] Although the network of Mo_9 clusters in $Ag_xMo_9Se_{11}$ differs from that characterizing the three above-mentioned compounds, inter-cluster distances are similar to those encountered in $Ag_{4.1}ClMo_9Se_{11}$ and $Ag_{2.6}CsMo_9Se_{11}$. Therefore, one can assume weak inter-cluster interactions in $Ag_xMo_9Se_{11}$ as well and the presence of monovalent Ag^+ cations with a semiconducting behaviour predicted to develop for $x = 4$.

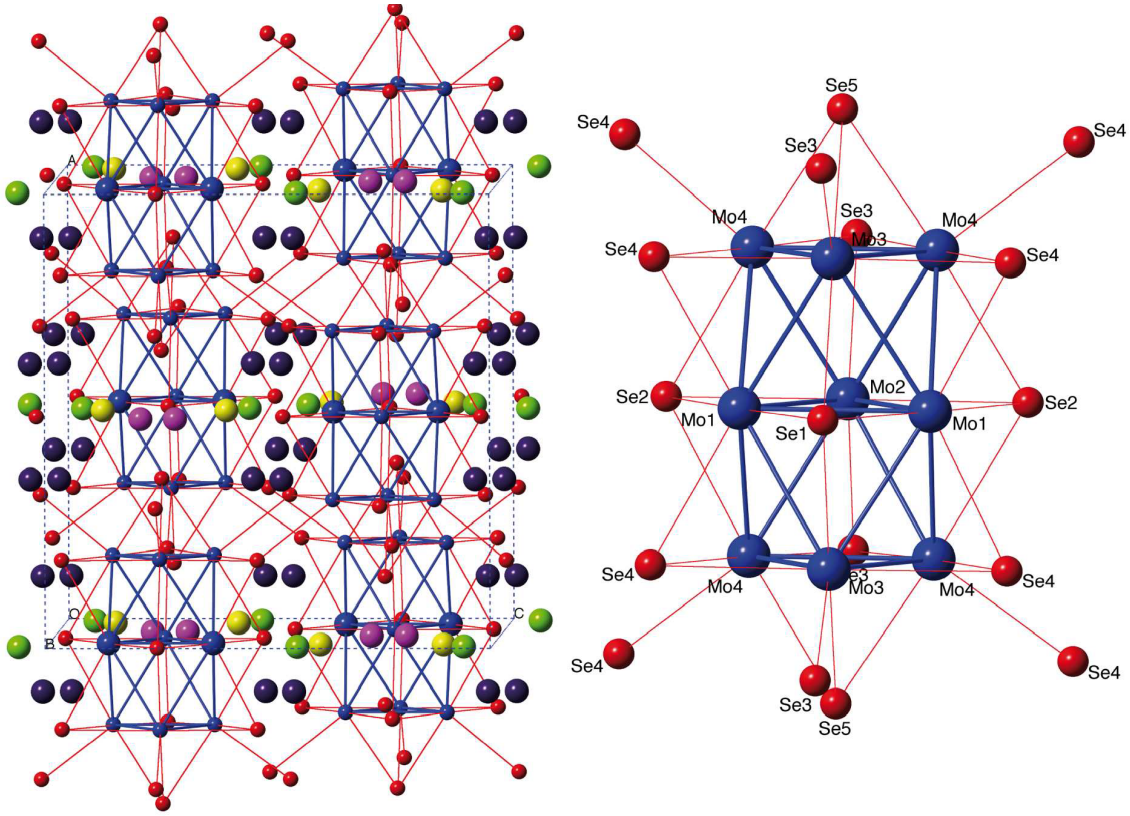

Fig. 1 Crystal structure of the $Ag_xMo_9Se_{11}$ compounds (left) highlighting the four crystallographic positions of Ag atoms: Ag1 (yellow sphere), Ag2 (green sphere), Ag3

(purple sphere) and Ag4 (navy blue sphere); $Mo_9Se^{i}_{4}Se^{a}_{4}$ cluster (right). Letters *i* and *a* stand for *inner* and *apical*, respectively.

Table 1. Positional parameters of Ag in $Ag_{3.6}Mo_9Se_{11}$ determined by single-crystal X-ray diffraction experiments.[34]

Atom position	Wyckoff notation	*x*	*y*	*z*	SOF[a]
Ag1	8*f*	0	0.1328	0.3886	0.806
Ag2	8*f*	0	0.0610	0.0629	0.212
Ag3	8*f*	0	0.4253	0.2109	0.508
Ag4	16*h*	0.3725	0.9924	0.4679	0.138

[a] Site occupancy factor

In order to verify this last assumption using quantum chemical tools, one must first model the crystal structure of $Ag_xMo_9Se_{11}$ that takes into account the fractional occupations on the Ag sites (Table 1). Such a model can be based on a supercell description of the crystal structure of $Ag_{3.6}Mo_9Se_{11}$ characterized by X-ray diffractions experiments with a random occupation of Ag positions consistent with the $Ag_4Mo_9Se_{11}$ stoichiometry. However, this approach has a major drawback: computing the band structure of models with large unit cell is time-consuming. In the case of $Ag_{3.6}Mo_9Se_{11}$, the low symmetry of the crystal structure and the substantial unit cell volume (≈ 1893 $Å^3$) make it difficult to compute the electronic band structure of a model based on a supercell approach with high accuracy. In order to implement less time-consuming models, the electronic band structure of an $Ag_4Mo_9Se_{11}$ model with the same space group can be undertaken assuming some hypotheses and approximations for the Ag positions. The first approximation is related to the Ag1 and Ag2 sites which are too close to each other to be occupied simultaneously. In addition, if the Ag2 site is occupied, the distance between the two Ag atoms occupying this site is only 2.217 Å. To avoid such a short and unrealistic distance, the Ag2 site has been moved to the (0, 0, 0) position, decreasing its multiplicity from 8 to 4. A similar situation occurs for the Ag3 and Ag4 atoms. Because of the

presence of mirror planes, the Ag3 sites are only separated by 0.913 Å and the shortest Ag4-Ag4 distance is equal to 0.778 Å. Thus, in order to keep the *Cmcm* space group, the Ag3 and Ag4 sites have been moved to (0, 0.4253, ¼) and (0.3725, 0, ½), respectively. These translations divide by two the multiplicity of these sites. The resulting multiplicity of the Ag4 site is equal to 8 (similar to Ag1) while that of Ag2 and Ag3 is reduced to 4. The environments of silver atoms both in the X-ray and model structures are depicted in Figure S1 (Supporting Information).

Thanks to these changes, we used two models to compute the electronic band structure of $Ag_4Mo_9Se_{11}$ starting from the crystal structure determined by X-ray diffraction. The electronic band structure calculated considering only the Ag1 and Ag4 sites as occupied (model **1**) is sketched in Fig. 2. Since $Ag_4Mo_9Se_{11}$ is expected to be semiconducting, the mBJ exchange-correlation functional was used to overcome the problem of underestimation of the band gaps inherent to the LDA and GGA functionals. Because of the presence of 4*d* elements in the compounds, relativistic effects can play a significant role in the calculations. Thus, the band structure was also computed using the same functional and including spin-orbit interaction. Both electronic band structures (Fig. 2a and Fig. S2, Supporting Information) are very similar indicating that relativistic effects hardly modify the band structure of these compounds, at least in the vicinity of the Fermi level. It is noteworthy that transport properties are mainly governed by the bands located at the top of the valence band and those lying at the bottom of the conduction band. As already shown by some of us, the bands around the Fermi level are mainly centred on Mo atoms, and to a lesser extent on Se atoms.[43] The presence of flat bands in some directions shows that few interactions occur in the crystal structure in these directions, revealing that cluster units hardly interact in the solid state. On the contrary, some bands are rather dispersive, especially is the Y→Γ direction. This corresponds to the direction of Mo-Se bonds that connect the bioctahedral clusters in the crystal structure. The bands

located at the bottom of the conduction band, mainly centered on Mo3 and Mo4 atoms,[43] exhibit a strong Mo-Mo antibonding character. Therefore, assuming a rigid band model, the upper limit of the Ag content in $Ag_xMo_9Se_{11}$ seems to be achieved for $x = 4$.

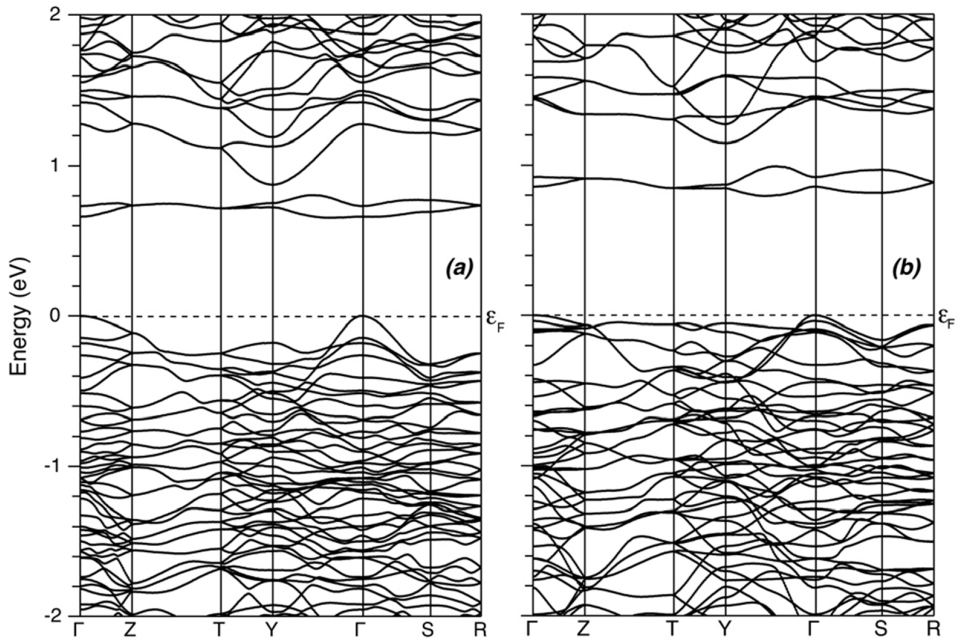

Fig. 2 Band structures of models **1** (a) and **2** (b) of $Ag_4Mo_9Se_{11}$ computed using the mBJ functional without taking into account spin-orbit coupling. Coordinates of high symmetry k-points: Γ = (0, 0, 0), Z = (0, 0, ½), T = (-½, ½, ½) , Y = (-½, ½, 0), S = (0, ½, 0), and R = (0, ½, ½).

In order to evaluate the effect of Ag on the electronic band structure of $Ag_xMo_9Se_{11}$, another structural model with the same chemical formula $Ag_4Mo_9Se_{11}$ was considered. This second model, referred to as model **2** hereafter, is based on the X-ray crystal structure of $Ag_{3.6}Mo_9Se_{11}$ where the Ag2, Ag3 and Ag4 sites are occupied. The corresponding band structure is sketched in Fig. 2b. From a qualitative point of view, both models lead to similar results. Nevertheless, the band gap is nearly 0.20 eV larger in model **2** than in model **1**. Upon closer inspection of these band structures, some differences in the band energies are visible in

almost all directions of the Brillouin zone. Since the electronic transport properties are computed from the band curvatures, these differences are expected to lead to variations in the computed transport properties. Flat bands are present at the top of the valence band and at the bottom of the conduction band in both cases. On one hand, this feature suggests that the density-of-state effective mass of the charge carriers should be high indicating that large thermopower values are achievable. On the other hand, the presence of dispersive bands around ε_F in both models suggests a high mobility of the charge carriers and a good electrical conductivity.

The electronic transport properties were computed for the two models of $Ag_4Mo_9Se_{11}$ using the semi-classical approach. The electrical conductivity divided by the constant relaxation time and the thermopower as a function of the chemical potential are shown in Fig. 3. Assuming a constant relaxation time, the electrical conductivities are almost similar for both models regardless of the chemical potential and the temperature. In contrast, the maximum thermopower value is more than twice higher at 300 K than that computed at 800 K. However, for the charge carrier estimated for $Ag_4Mo_9Se_{11}$ (*vide infra*), the thermopower is computed slightly larger at 800 K than at room temperature. This trend roughly agrees with the experimental data for which the σ values approach 80 and 180 μV/K at 300 and 800 K, respectively, for $Ag_{3.9}Mo_9Se_{11}$. At both temperatures, the maximum thermopower value for *p*-type doping is significantly larger than that obtained for *n*-type doping. It is important to mention that the main carriers are holes in cluster-based molybdenum chalcogenides, at least at high temperatures.[1-3,9-14,43] From a qualitative point of view, the curves of the properties computed for models **1** and **2** almost follow the same trends. Nevertheless, subtle differences can become very significant when quantitative estimations are envisioned: using the charge carrier concentrations obtained from Hall effect measurements, one can estimate the relaxation time by comparing the experimental and computed electrical conductivities. In the

case of $Ag_xMo_9Se_{11}$, the charge carrier concentration was estimated to be 1.9×10^{20} cm^{-3} at 300 K for $x = 3.78$. Using this value, the relaxation time was estimated between 300 and 800 K with steps of 100 K. For models **1** and **2**, the averaged τ is estimated to be 4.0×10^{-15} and 1.1×10^{-14} s, respectively. The corresponding standard deviations, that equal to 1.0×10^{-16} s and 1.3×10^{-15} s, respectively, are rather low indicating that these estimations hardly depend on the temperature. These results confirm the difficulty to quantitatively estimate the electrical conductivity within this approach owing to the sensitivity to the structural model considered, among other parameters.

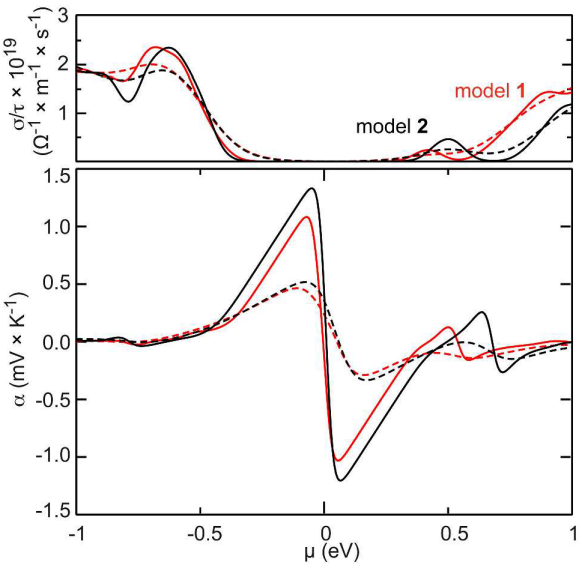

Fig. 3 Electrical conductivity (σ/τ) and Seebeck coefficient (σ) computed as a function of chemical potential (μ) for $Ag_4Mo_9Se_{11}$ models at 300 K (plain) and 800 K (dotted).

To go further, cell parameters and atomic positions were relaxed with respect to energy. The main interatomic distances are reported in Table 2. In addition to models **1** and **2**, a third model (model **3**) was considered where the Ag1, Ag2 and Ag3 positions are occupied. Mo-Mo distances in optimized and nonoptimized structures deviate less than 0.05 Å, except for

the Mo4-Mo4 intra-triangle distance in model **1**. Indeed, even if slight differences appear between the three models, the averaged Mo-Mo distances within the Mo_9 cluster are very similar: 2.689 Å, 2.693 Å, and 2.696 Å, for models **1**, **2** and **3**, respectively. These values compare very well with the Mo-Mo distances in the nonoptimized models **1** and **2** that are equal to 2.700 Å. Optimized Ag-Se distances differ more significantly from those in the nonoptimized models. This discrepancy originates from the shift of silver positions in the model structure of $Ag_4Mo_9Se_{11}$ (*vide supra*). The large variations in Ag-Se distances that are observed for some models demonstrate the versatility of these bonds, in agreement with the large anisotropic thermal displacement parameters measured for the Ag atoms in the crystal structure.[34]

The electronic band structures of the optimized models of $Ag_4Mo_9Se_{11}$ are sketched in Fig. 4. For all models, the bottom of the conduction band shows some flat bands that are separated from the other conduction bands by an energy gap that approximately varies from 0.2 to 0.4 eV. More significant changes occur at the top of the valence band. For instance, the highest band lying at Γ in models **1** and **3** is shifted at Y in model **2**. The electronic transport properties were computed from these band structures. The thermopower values were calculated as a function of temperature using the carrier concentration measured at 300 K for $Ag_{3.78}Mo_9Se_{11}$ (Fig. 5). The values computed for the three optimized models lie within a maximum range of 20 μV/K and fall between the ones computed for the nonoptimized models. These results demonstrate that optimizing different structural parameters of the crystal structure of these compounds leads to well converged thermopower values. Moreover, our calculations only slightly overestimate the experimental data.

The temperature dependence of the thermoelectric figure of merit *ZT* is shown in Fig. 5. *ZT* was computed for all models using the experimental total thermal conductivity. For the electrical conductivity, as previously described in this work, the relaxation time was

determined for each model by comparison of the computed σ/τ value with the electrical conductivity measured for $Ag_{3.9}Mo_9Se_{11}$. In the case of the optimized models, τ is estimated to be 5.4×10^{-15} s, 6.9×10^{-15} s, and 8.9×10^{-15} s, for models **1**, **2** and **3**, respectively. The overestimation of the computed thermopower is at the origin of the differences observed in the theoretical *ZT* values.

Table 2 Main interatomic distances (Å) optimized for the different structural models of $Ag_3Mo_9Se_{11}$ and $Ag_4Mo_9Se_{11}$ compared with $Ag_{3.6}Mo_9Se_{11}$.[34]

Models	$Ag_4Mo_9Se_{11}$			$Ag_3Mo_9Se_{11}$			$Ag_{3.6}Mo_9Se_{11}$
	1	**2**	**3**	**4**	**5**	**6**	X-ray
Mo1-Mo1	2.748	2.703	2.774	2.697	2.683	2.786	2.747
Mo1-Mo2	2.729	2.749	2.763	2.688	2.706	2.726	2.747
Mo3-Mo4	2.613	2.594	2.634	2.582	2.601	2.634	2.632
Mo4-Mo4	2.590	2.622	2.648	2.655	2.588	2.666	2.663
Mo1-Mo3	2.734	2.720	2.721	2.679	2.709	2.714	2.731
Mo1-Mo4	2.713	2.716	2.688	2.694	2.708	2.653	2.690
Mo2-Mo4	2.713	2.747	2.714	2.757	2.729	2.709	2.729
Mo4-Mo4 inter Mo_9	3.764	3.735	3.759	3.530	3.604	3.561	3.727
Ag1-Se1	2.726		2.983			2.572	2.656
Ag1-Se4	2.792		2.955			2.735	2.767
Ag1-Se5	2.959		2.711			2.806	2.894
Ag2-Se1		2.977	3.036		2.822		2.459
Ag2-Se4		2.871	2.924		2.750		2.620
Ag3-Se3		2.825	2.779	2.775		2.755	2.809
Ag3-Se5		2.888	2.913	2.706		2.735	2.861
Ag4-Se2	2.793	2.781		2.693	2.673		2.559
Ag4-Se3	3.012	3.064		2.885	2.894		2.738
Ag4-Se4	2.799	2.800		2.697	2.795		2.737

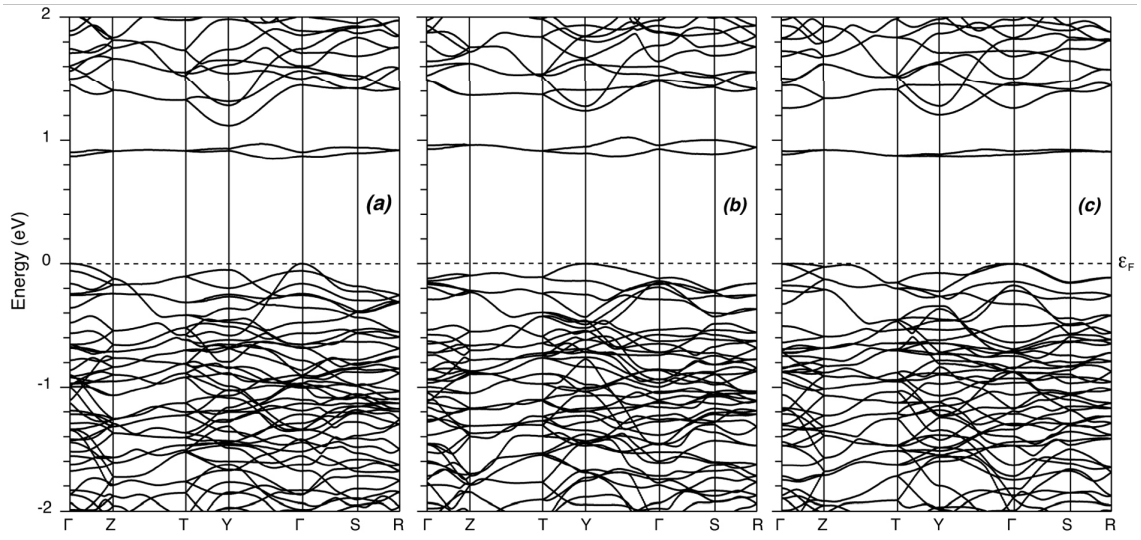

Fig. 4 Band structures of the optimized structure of models **1** (a), **2** (b), and **3** (c) of $Ag_4Mo_9Se_{11}$ computed using the mBJ functional without taking into account spin-orbit coupling.

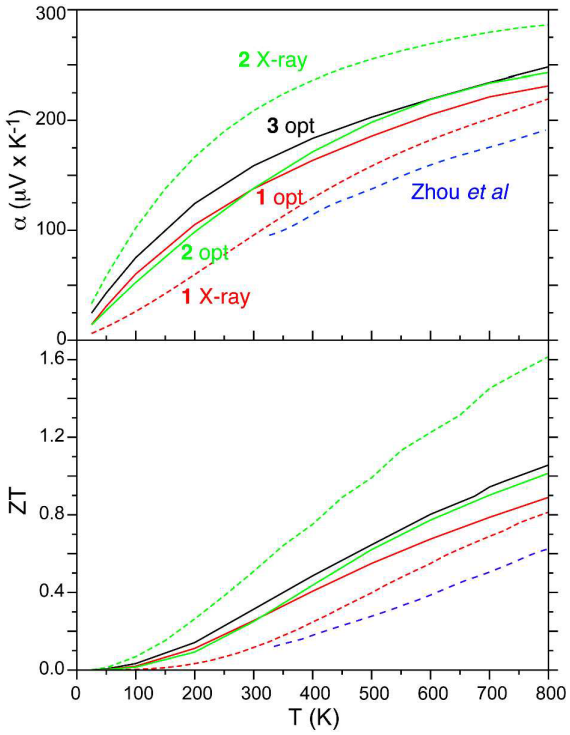

Fig. 5 Seebeck coefficient (α) (top) and figure of merit (ZT) (bottom) computed as a function of temperature for various models of $Ag_4Mo_9Se_{11}$.

These calculations demonstrate that our computational approach based on DFT band-structure calculations combined with a semi-classical approach can help to understand the transport properties of cluster-based materials and to predict the thermopower values with the necessary condition that the crystal structure has been formerly relaxed. In the case of the electrical conductivity, our calculations show that large discrepancies occur between σ/τ of the different models.

In order to study the influence of the Ag content, the transport properties were computed for different models of composition $Ag_3Mo_9Se_{11}$. Three models are labelled hereafter models **4**, **5**, and **6**. In model **4**, the Ag3 and Ag4 positions are occupied while the Ag2 and Ag4 sites are occupied in model **5**. In model **6**, the Ag1 and Ag3 sites are occupied. Cell parameters and atomic positions were relaxed within the *Cmcm* space group using the PBE functional. As for $Ag_4Mo_9Se_{11}$ models, Ag2, Ag3 and Ag4 positions were moved, as previously described in the paper. Main optimized distances are reported in Table 2. As for the $Ag_4Mo_9Se_{11}$ optimized models, some differences appear within the optimized Mo-Mo distances of the different models. The averaged Mo-Mo distances within the Mo_9 clusters are however almost equal, as for optimized $Ag_4Mo_9Se_{11}$ models. These averaged valued are *ca.* one hundredth of Å shorter than the ones optimized for $Ag_4Mo_9Se_{11}$ models. In contrast, Mo-Mo inter-cluster distances are much shorter for $Ag_3Mo_9Se_{11}$ than for $Ag_4Mo_9Se_{11}$. This is consistent with the relationship between the unit cell volume and the Ag filling rate.[43]

The thermopower as a function of chemical potential is shown in Fig. 6 for both models computed using PBE and mBJ functionals. In line with the DOS computed for $Ag_4Mo_9Se_{11}$ models, $Ag_3Mo_9Se_{11}$ is predicted to be metallic in character. This metallic character is consistent with the band structure of all $Ag_3Mo_9Se_{11}$ models, computed either with PBE of mBJ functionals, sketched in Fig. S4 (Supporting Information). Therefore, the use of the PBE-

GGA functional to compute transport properties was also evaluated. It is noteworthy that for each model, the thermopower computed using the mBJ functional is slightly shifted towards higher chemical potentials than those computed with the PBE one. This is consistent with the GGA underestimation of the band energy gap that is partly corrected using the mBJ functional. Moreover, for both models, the thermopower is found to be slightly higher using mBJ than PBE. It is noteworthy to mention that the higher the band gap, the higher the computed Seebeck: the band gap of model **5** is larger than the one of models **4** and **6**, that are similar. These values of the thermopower compare rather well with the ones computed at the same temperature for the $Ag_4Mo_9Se_{11}$ models (see Fig. 3), in agreement with the negligible contribution to the bands that govern the transport properties in this system which further justifies the rigid band approach. In addition, this shows that, for metallic systems, the PBE functional performs as well as an orbital-dependent potential such as that embedded in mBJ.[30]

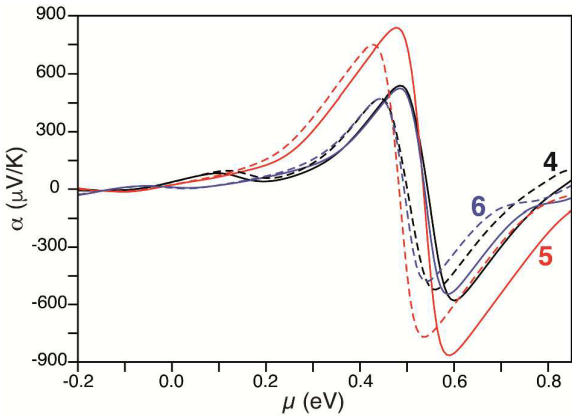

Fig. 6 Seebeck coefficient (α) computed as a function of chemical potential (μ) for $Ag_3Mo_9Se_{11}$ models at 300 K using PBE (dotted) and mBJ (plain) functionals.

3.2 $Ag_3In_2Mo_{15}Se_{19}$ and $Ag_{2.25}Tl_{1.75}Mo_9Se_{11}$

How far can this computational approach be extended to other Mo cluster-based compounds? To gain insights into this question, two additional compounds were considered, namely

$Ag_3In_2Mo_{15}Se_{19}$ and $Ag_{2.25}Tl_{1.75}Mo_9Se_{11}$. The crystal structure of the latter is also based on bioctahedral Mo_9 clusters.[12] Unlike $Ag_xMo_9Se_{11}$, this compound does not crystallize in the orthorhombic space group *Cmcm* but rather with a novel structure type of rhombohedral symmetry, successfully indexed in the *R*-3*c* space group. Each $Mo_9Se_{11}Se_6$ motif is connected to six adjacent units *via* 12 interunit Mo−Se bonds to form a three-dimensional Mo−Se framework in which the shortest inter-cluster distance is 3.6919(8) Å, that is similar to that encountered in $Ag_xMo_9Se_{11}$. $Ag_3In_2Mo_{15}Se_{19}$ is isostructural to $In_2Mo_{15}Se_{19}$ [44] and crystallizes in the *R*-3*c* space group.[13] In this compound, the Mo−Se framework is based on an equal mixture of Mo_9Se_{11} clusters and Mo_6Se_8 octahedral units interconnected through Mo-Se bonds, in a similar way to that present in $Ag_{2.25}Tl_{1.75}Mo_9Se_{11}$. Assuming a complete transfer of electrons from Ag and Tl towards the Mo-Se framework, the latter compound is expected to be semiconducting since a +1 oxidation state is considered for Tl atoms owing to their atomic environment. This prediction is consistent with the computed band structure and the measured resistivity of this compound.[12] In contrast, $Ag_3In_2Mo_{15}Se_{19}$ is expected to be metallic: the ME count of the Mo-Se framework is equal to 54 which is far from 60, *i.e.*, the sum of the optimal ME counts of 24 and 36 for Mo_6Se_8 and Mo_9Se_{11} clusters, respectively, required to achieve a semiconducting state. This ME count suggests that the valence band is partially filled. Although somewhat complex at low temperatures, $Ag_3In_2Mo_{15}Se_{19}$ exhibits metallic properties above 100 K.[13] Band structure calculations are consistent with this behaviour.

The transport properties of both compounds have been computed within the semi-classical approach using band structure calculations. Band structures of $Ag_2Tl_2Mo_9Se_{11}$ and $Ag_3In_2Mo_{15}Se_{19}$ (not shown here) are consistent with those reported in prior studies.[12,13] Because of the presence of the two types of carriers in both $Ag_2Tl_2Mo_9Se_{11}$ and $Ag_3In_2Mo_{15}Se_{19}$, the hole concentration was not determined from the measurement of the Hall

coefficient. Thus, the thermopower was computed as a function of temperature for two different carrier concentrations (Fig. 7). All the values are found to be positive, except for $Ag_3In_2Mo_{15}Se_{19}$ at low temperatures. Such behaviour is consistent with the presence of a pseudo-gap below ε_F favouring electrons as the main charge carriers at low temperatures. As the temperature increases, hole conduction increases and become the dominant population of charge carriers. These results are consistent with the experimental data obtained on these two compounds. The Seebeck coefficients computed for $Ag_3In_2Mo_{15}Se_{19}$ are smaller, as expected from the more pronounced metallic character expected for this compound compared to semiconducting Mo_9-based compounds. Regardless of the dominant type of charge carriers, the thermopower values computed for $Ag_2Tl_2Mo_9Se_{11}$ are larger than those computed for $Ag_4Mo_9Se_{11}$. This difference stems from the electronic band structure of $Ag_2Tl_2Mo_9Se_{11}$ [12] that shows a higher band degeneracy at the top of the valence band than those computed for the $Ag_xMo_9Se_{11}$ models.

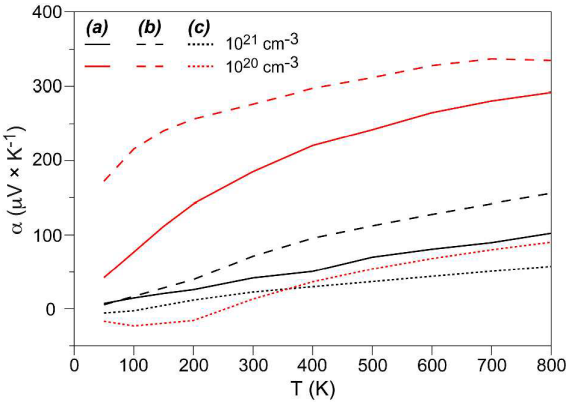

Fig. 7 Seebeck coefficient (α) computed for different carrier concentrations as a function of temperature for (a) $Ag_4Mo_9Se_{11}$ (solid), (b) $Ag_2Tl_2Mo_9Se_{11}$ (dashed) and (c) $Ag_3In_2Mo_{15}Se_{19}$ (dotted) models.

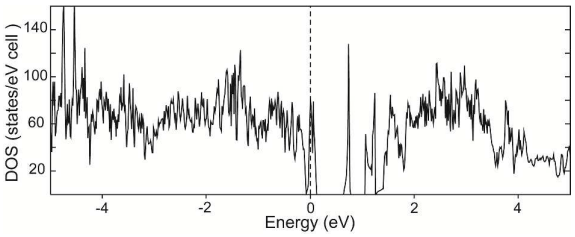

Fig. 8 DOS for $Ag_3In_2Mo_{15}Se_{19}$.

4 Conclusion

The transport properties of three cluster-based molybdenum selenides have been studied within a semi-classical approach using DFT band structure calculations. Different structural models with respect to the Ag atomic positions were considered for $Ag_xMo_9Se_{11}$. Even though the model of the crystal structure considered strongly influences the computed properties, relaxation of the cell parameters and atomic positions reduces the differences between calculations and experiments, at least for the thermopower. The results hardly change with respect to the stoichiometry considered for the structural model of $Ag_xMo_9Se_{11}$ which justifies a rigid band approach often considered for these cluster compounds. The computational study was extended to two additional compounds, $Ag_2Tl_2Mo_9Se_{11}$ that is also based on Mo_9 motifs, and $Ag_3In_2Mo_{15}Se_{19}$ the crystal structure of which contains both octahedral Mo_6 and bioctahedral Mo_9 clusters. For the thermopower, a trend similar to that observed experimentally was found. Because the number of known cluster-based materials is numerous, experimental screening of their transport properties might be difficult. Our results suggest that a computational approach constitute a useful alternative to predict their transport properties, potentially leading to the identification of candidates of interest for thermoelectric applications at high temperatures.

Conflicts of interest

There are no conflicts to declare.

Acknowledgements

B. B. acknowledges support from Région Bretagne (France) and the Max Planck Society (Germany) for a Ph. D. grant.

References

1. T. Caillat, and J.-P. Fleurial, *J. Phys. Chem. Solids*, 1998, **6-7**, 1139-1144.
2. T. Caillat, J.-P. Fleurial, and G. J. Snyder, *Solid State Sci.*, 1999, **1**, 535-544.
3. T. Tsubota, M. Ohtaki, and K. Eguchi, *J. Ceram. Soc. Jpn.*, 1999, **197**, 697-701.
4. M. A. McGuire, A. M. Schmidt, F. Gascoin, G. J. Snyder, and F. J. DiSalvo, *J. Solid State Chem.*, 2016, **179**, 2158-2163.
5. A. M. Schmidt, M. A. McGuire, F. Gascoin, G. J. Snyder, and F. DiSalvo, *J. Alloys Compd.*, 2007, **431**, 262-268.
6. M. Ohta, H. Obara, and A. Yamamoto, *Mater. Trans.*, 2009, **50**, 2129-2133.
7. H. Nishiate, M. Ohta, A. Yamamoto, H. Obara, C.-H. Lee, and K. Ueno, *Mater. Trans.*, 2011, **52**, 1535-1538.
8. R. Chevrel, and M. Sergent, in *Superconductivity in Ternary Compounds I*, Topics of Current Physics Vol. 32, ed. Ø. Fischer and M. B. Maple, Springer, Berlin, Heidelberg, 1982, pp. 25–86.
9. T. Zhou, B. Lenoir, M. Colin, A. Dauscher, R. Al Rahal Al Orabi, P. Gougeon, M. Potel, and E. Guilmeau, *Appl. Phys. Lett.*, 2011, **98**,162106.
10. T. Zhou, B. Lenoir, C. Candolfi, A. Dauscher, P. Gall, P. Gougeon, M. Potel, and E. Guilmeau, *J. Electron. Mater.,* 2011, **40**, 508-512.
11. M. Colin, T. Zhou, B. Lenoir, A. Dauscher, R. Al Rahal Al Orabi, P. Gougeon, M. Potel, P. Baranek, and C. Semprimoschnig, *J. Electron. Mater.*, 2012, **41**, 1360-1364.
12. R. Al Rahal Al Orabi, P. Gougeon, P. Gall, B. Fontaine, R. Gautier, M. Colin, C. Candolfi, A. Dauscher, J. Hejtmanek, B. Malaman, and B. Lenoir, *Inorg. Chem.*, 2014, **53**, 11699-11709.
13. P. Gougeon, P. Gall, R. Al Rahal Al Orabi, B. Fontaine, R. Gautier, M. Potel, T. Zhou, B. Lenoir, M. Colin, C. Candolfi, and A. Dauscher, *Chem. Mater.*, 2012, **24**, 2899–2908.
14. R. Al Rahal Al Orabi, B. Fontaine, R. Gautier, P. Gougeon, P. Gall, Y. Bouyrie, A. Dauscher, C. Candolfi, and B. Lenoir, *Inorg. Chem.*, 2016, **55**, 6616-6624.
15. D. J. Singh and I. Terasaki, *Nat. Mater.*, 2008, **7**, 616-617
16. T. Mori, *Small*, 2017, 1702013.
17. C. Perrin, *J. Alloys Compd.*, 1997, **262-263**, 10-21.
18. A. Simon, in *Clusters and Colloids. From Theory to Applications,* ed. G. Schmid, VCH, Weinheim, 1994, pp 373-458.

19. H. Zhu, W. Sun, R. Armiento, P. Lazic, and G. Ceder, *Appl. Phys. Lett.*, 2014, **104**, 082107-5.
20. J. Li, M. Zhu, D. L. Abernathy, X. Ke, D. T. Morelli, and W. Lai, *APL Mater.*, 2016, **4**, 104811-6.
21. J. Shuai, H. Geng, Y. Lan, Z. Zhu, C. Wang, Z. Liu, J. Bao, C.-W. Chu, J. Sui, and Z. Ren, *Proc. Natl. Acad. Sci. U. S. A.*, 2016, **113**, 4125-4132.
22. K. P. Ong, D. J. Singh, and P. Wu, *Phys. Rev. B: Condens. Matter Mater. Phys.*, 2011, **83**, 115110.
23. C. Bera, S. Jacob, I. Opahle, N. S. H. Gunda, R. Chmielowski, G. Dennler, and G. K. H. Madsen, *Phys. Chem. Chem. Phys.*, 2014, **16**, 19894–19899.
24. J. Yan, P. Gorai, B. Ortiz, S. Miller, S. A. Barnett, T. Mason, V. Stevanovic, and E. S. Toberer, *Energy Environ. Sci.*, 2015, **8**, 983-994.
25. R. Al Rahal Al Orabi, J. Hwang, C.-C. Lin, R. Gautier, B. Fontaine, W. Kim, J.-S. Rhyee, D. Wee, and M. Fornari, *Chem. Mater.*, 2017, **29**, 612-620.
26. S. Bhattacharya, and G. K. H. Madsen, *Phys. Rev. B: Condens. Matter Mater. Phys.*, 2015, **92**, 085205-9.
27. W. Chen, J.-H. Pöhls, G. Hautier, D. Broberg, S. Bajaj, U. Aydemir, Z. M. Gibbs, H. Zhu, M. Asta, G. J. Snyder, B. Meredig, M. A. White, K. Persson, and A. Jain, *J. Mater. Chem. C*, 2016, **4**, 4414-4426.
28. P. Blaha, K. Schwarz, G. K. H. Madsen, D. Kvasnicka, and J. Luitz, WIEN2k 14.2, Vienna, Austria, 2011.
29. J. P. Perdew, K. Burke, and M. Ernzerhof, *Phys. Rev. Lett.*, 1996, **77**, 3865-3868.
30. F. Tran, and P. Blaha, *Phys. Rev. Lett.*, 2009, **102**, 226401-4.
31. T. J.Scheidemantel, C. Ambrosch-Draxl, T. Thonhauser, J. V. Badding, and J. O. Sofo, *Phys. Rev. B: Condens. Matter Mater. Phys.*, 2003, **68**, 125210.
32. G. K. H. Madsen, *J. Am. Chem. Soc.*, 2006, **128**, 12140–12146.
33. G. K. H. Madsen and D. J. Singh, *Comput. Phys. Commun.*, 2006, **175**, 67–71
34. P. Gougeon, J. Padiou, J.-Y. Le Marouille, M. Potel, and M. Sergent, *J. Solid State Chem.*, 1984, **51**, 218-226.
35. T. Hughbanks and R. Hoffmann, *J. Am. Chem. Soc.*, 1983, **105**, 1150-1162.
36. R. Gautier, P. Gougeon, J.-F. Halet, M. Potel, and J.-Y. Saillard, *J. Alloys Compd.*. 1997, **262-263**, 311-315.
37. S. Picard, J.-F. Halet, P. Gougeon, and M. Potel, *Inorg. Chem.*, 1999, **38**, 4422-4429

38. S. Picard, J.-Y. Saillard, P. Gougeon, H. Noël, and M. Potel, *J. Solid State Chem.*, 2000, **155**, 417-426.
39. P. Gougeon, M. Potel, and R. Gautier *Inorg. Chem.*, 2004, **43**, 1257-1263.
40. D. Salloum, R. Gautier, P. Gougeon, and M. Potel, *J. Solid State Chem.*, 2004, **177**, 1672-1680.
41. D. Salloum, P. Gougeon, M. Potel, and R. Gautier, *C. R. Chim.*, 2005, **11-12**, 1743-1749.
42. P. Gougeon, P. Gall, R. Gautier, and M. Potel, *Acta Crystallogr., Sect. C: Cryst. Struct. Commun.*, 2010, **C66**, i67.
43. T. Zhou, M. Colin, C. Candolfi, C. Boulanger, A. Dauscher, E. Santava, J. Hetjmanek, P. Baranek, R. Al Rahal Al Orabi, M. Potel, B. Fontaine, P. Gougeon, R. Gautier, and B. Lenoir, *Chem. Mater.*, 2014, **26**, 4765-4775
44. M. Potel, P. Gougeon, and M. Sergent, *Acta Cryst.*, 1981, **B37**, 1007-1010.

Table of Contents Entry

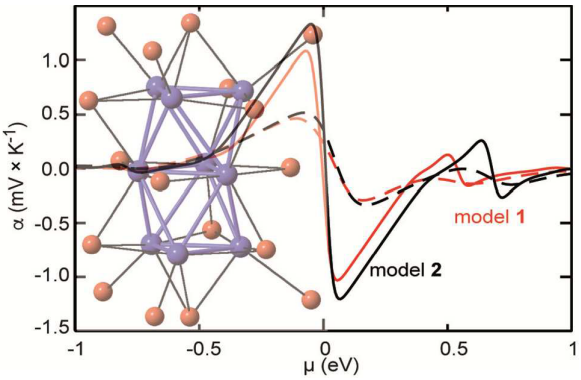

Supporting Information

Towards the Prediction of the Transport Properties of Cluster-Based Chalcogenides?

Rabih Al Rahal Al Orabi, Benoît Boucher, Bruno Fontaine, Philippe Gall,

Christophe Candolfi, Bertrand Lenoir, Patrick Gougeon, Jean-François Halet and

Régis Gautier*

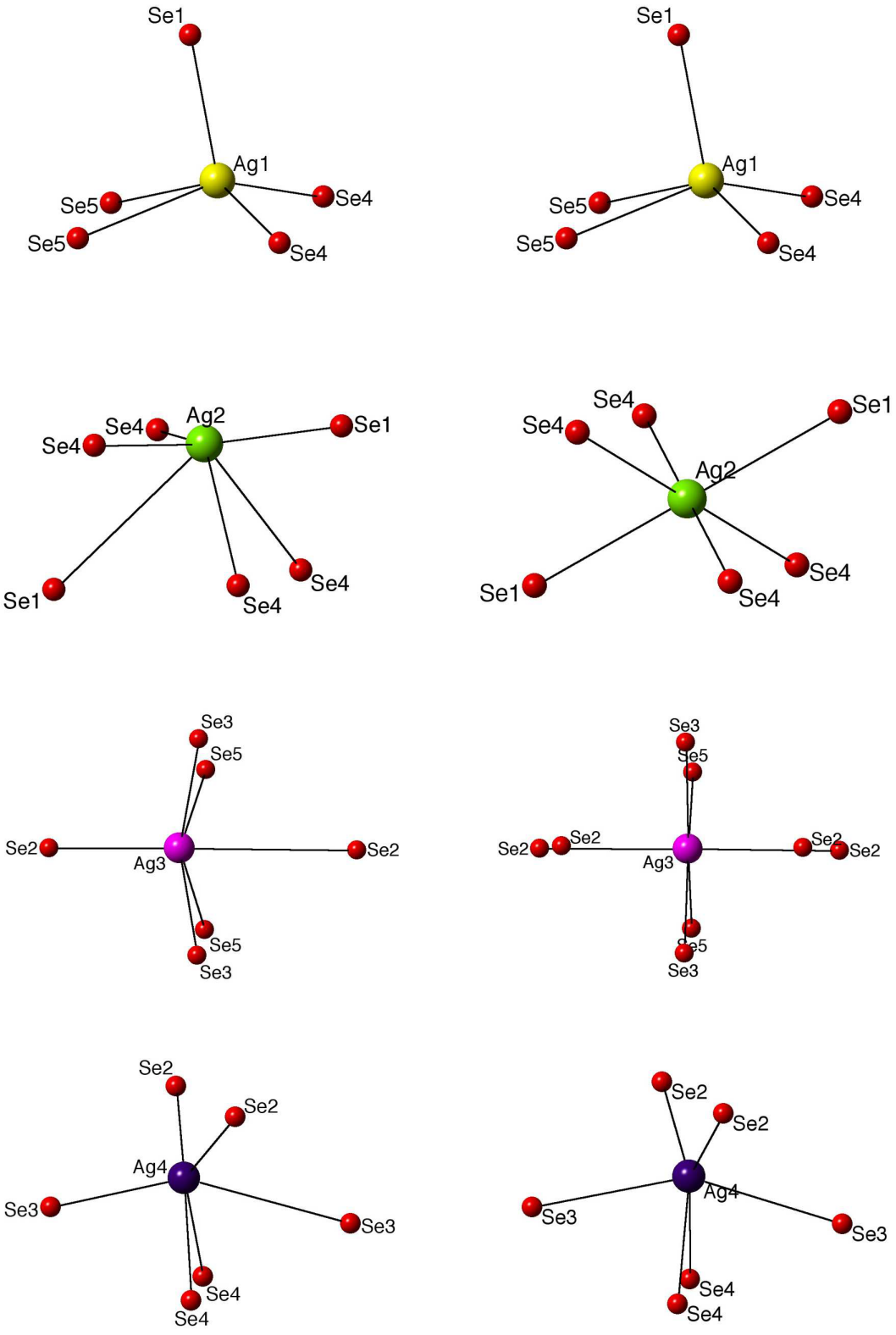

Fig. S1 Environments of Ag atoms in the X-ray structure (left) and models (right).

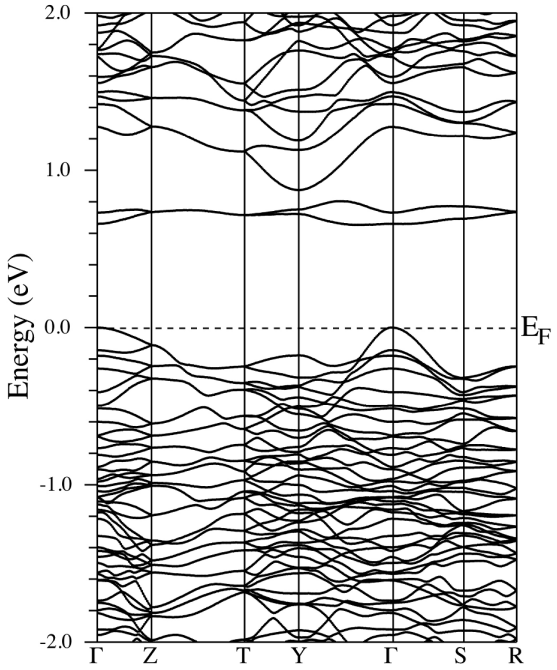

Fig. S2 Band structure of the model **1** of $Ag_4Mo_9Se_{11}$ computed using the mBJ functional and taking into account spin-orbit interaction.

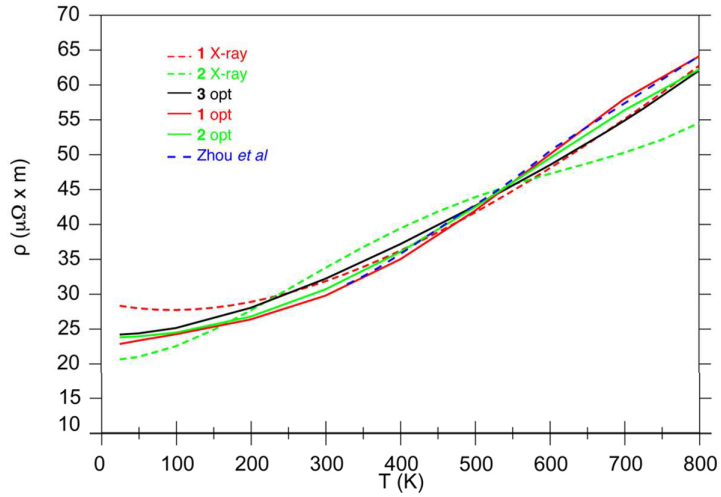

Fig. S3 Electrical resistivity ρ *vs* T computed for $Ag_4Mo_9Se_{11}$ models and compared with experimental measurements. The relaxation time is fitted in order that the averaged electrical conductivities resulting from measurements and BTE calculations match.

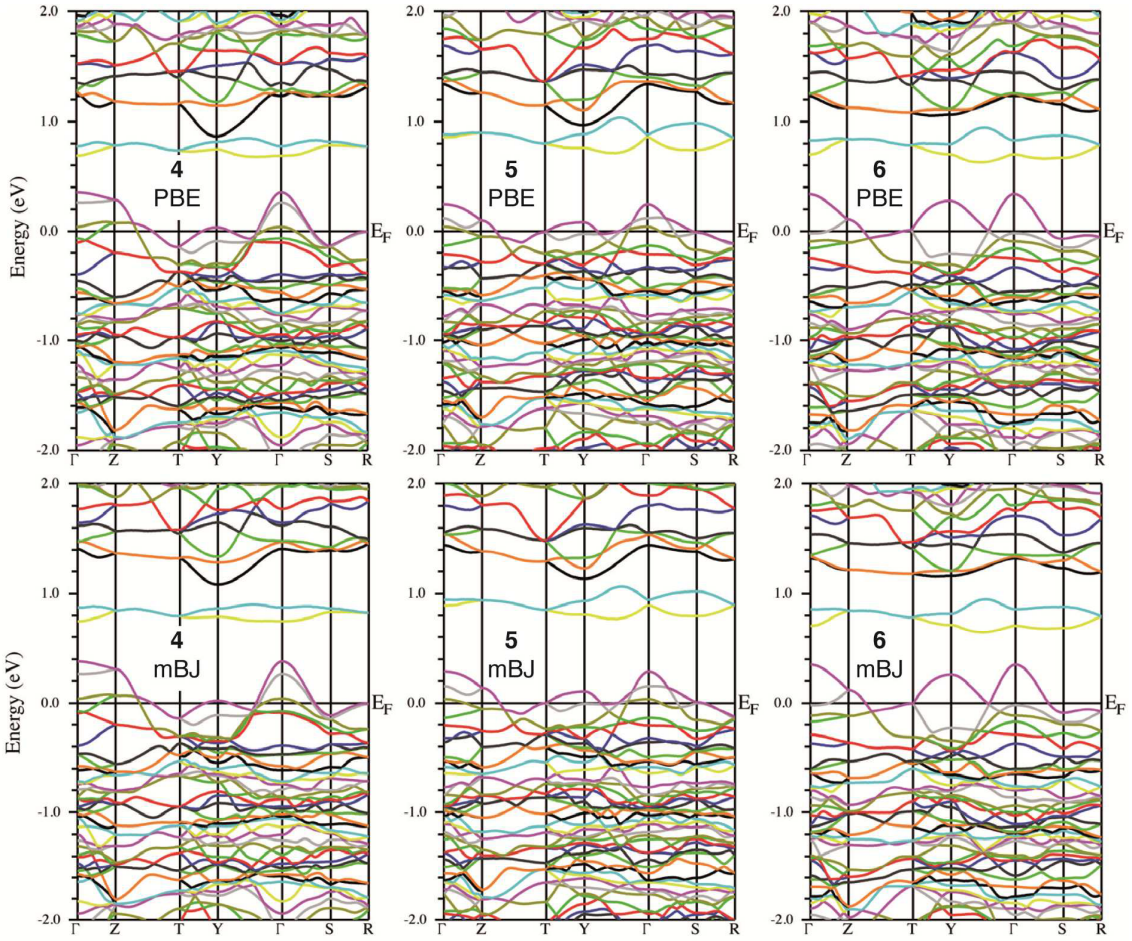

Fig. S4 PBE and mBJ band structures of $Ag_3Mo_9Se_{11}$ models.